Supplement of Atmos. Meas. Tech., 13, 3957–3975, 2020
https://doi.org/10.5194/amt-13-3957-2020-supplement

Atmospheric Measurement Techniques
Open Access
EGU

Supplement of

Towards standardized processing of eddy covariance flux measurements of carbonyl sulfide

Kukka-Maaria Kohonen et al.

Correspondence to: Kukka-Maaria Kohonen (kukka-maaria.kohonen@helsinki.fi)

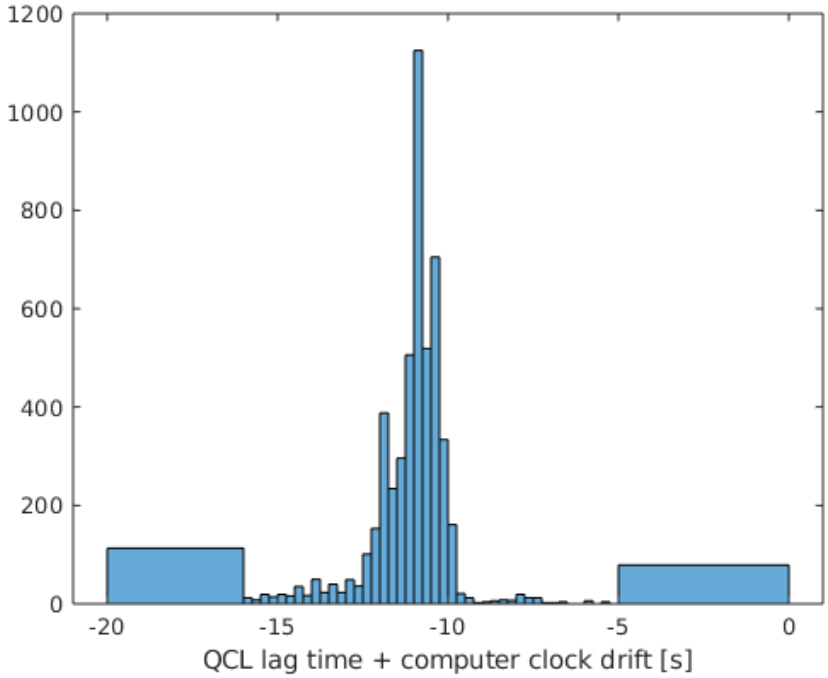

Figure S1. Histogram of the combined lag time of QCL lag and computer drift when combining files. The combined lag is determined from the maximum covariance of CO_2 (QCL) and *w*.

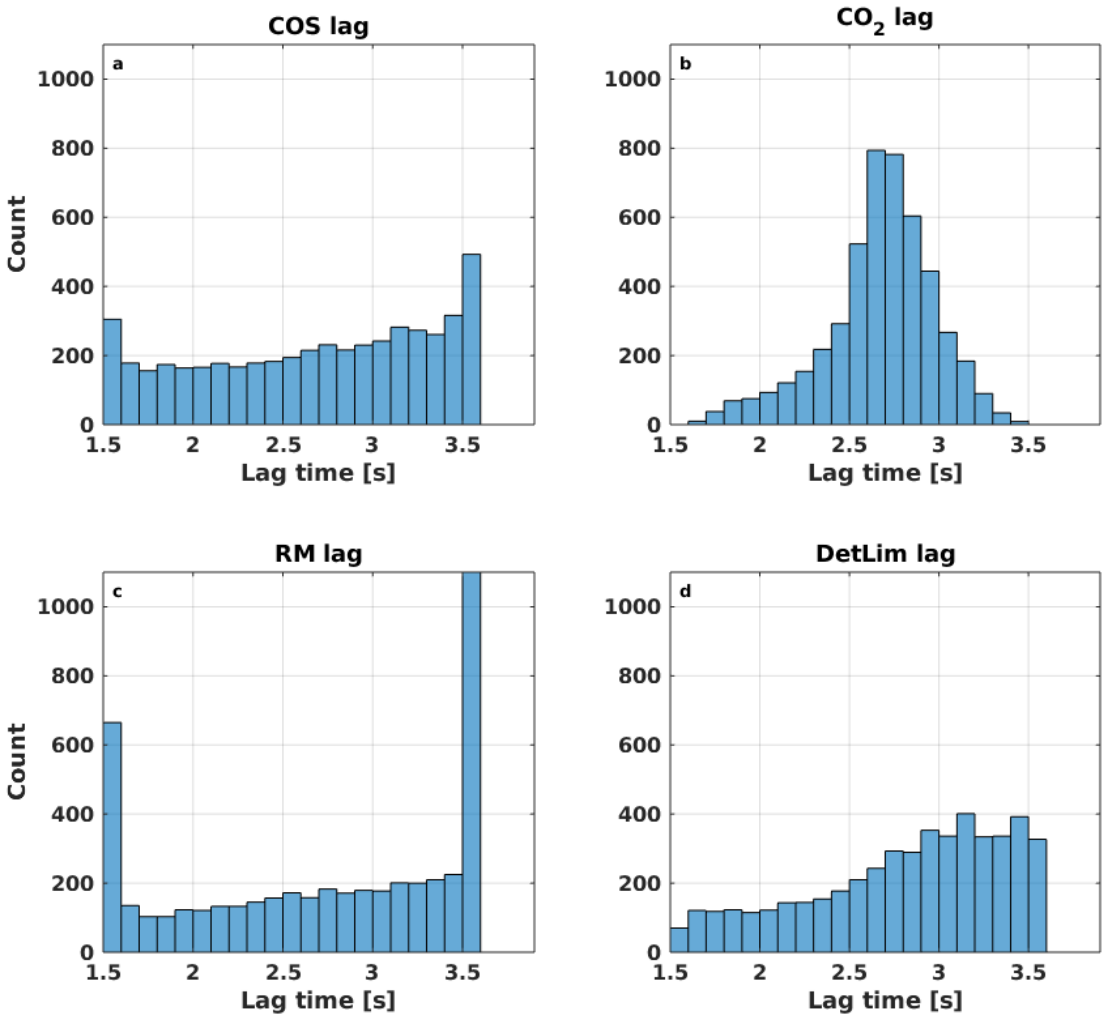

Figure S2. Distribution of lag times derived from different methods: COS lag (a), CO_2 lag (b), COS lag from a running mean cross-covariance (RM lag, c) and combination of COS and CO_2 lag times (DetLim lag, d), when all lag times were determined from the absolute cross-covariance maximum inside the lag window.

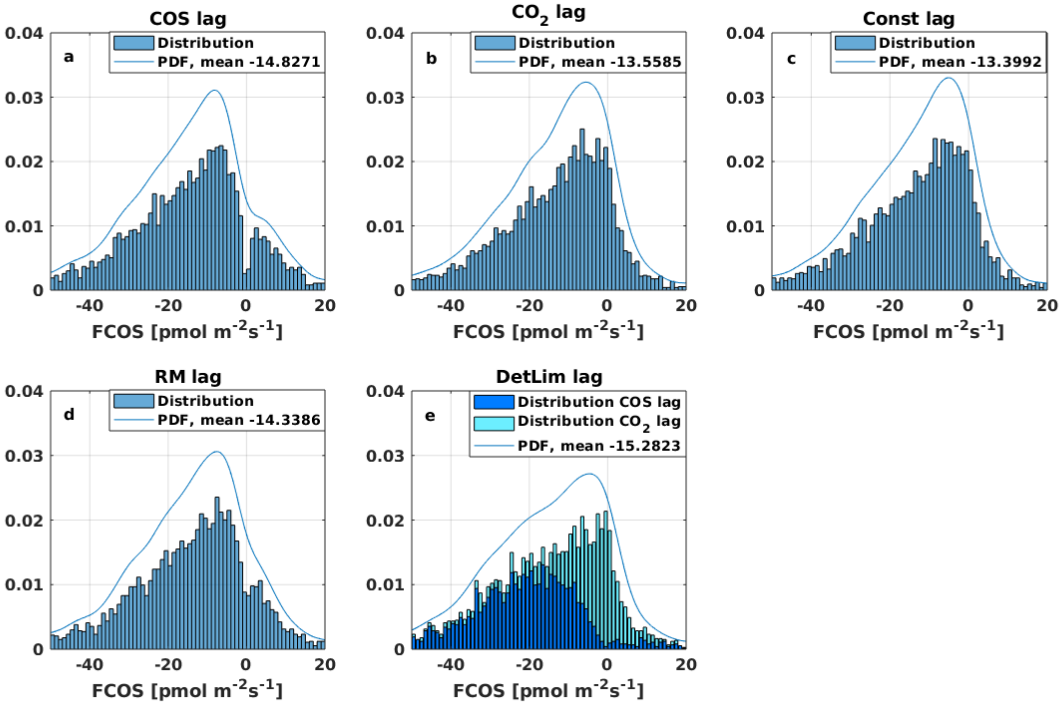

Figure S3. Normalized COS flux distributions using different lag time methods: COS lag (a), CO_2 lag (b), constant lag time of 2.6 s (c), lag time from a running mean COS cross-covariance (RM lag, d) and combination of COS and CO_2 lag times (DetLim lag, e), and a summary of all probability distribution functions (PDFs) (f), when lag times were determined from the absolute cross-covariance maximum inside the lag window.

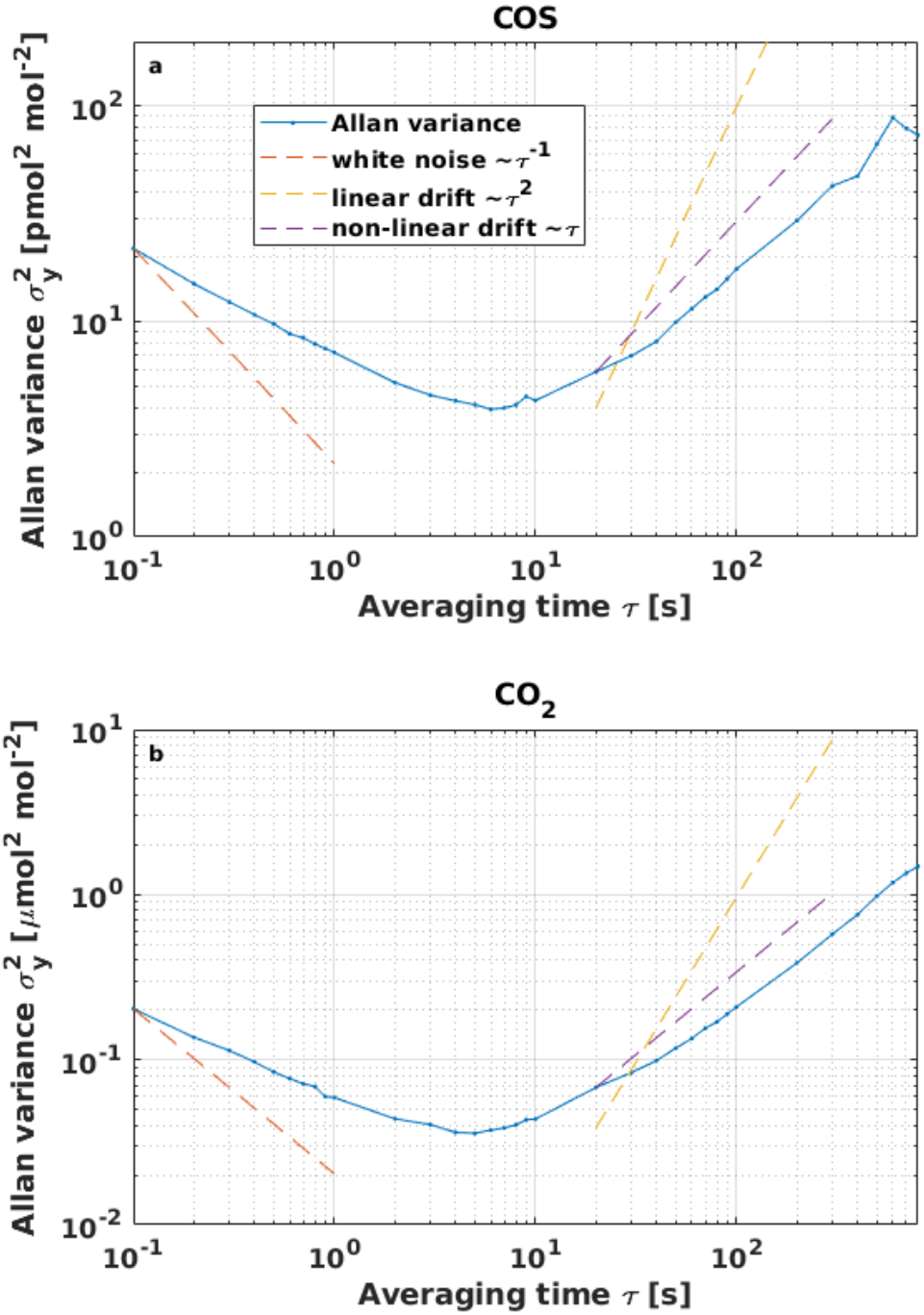

Figure S4. Allan variance plot for COS (a) and CO_2 (b) mixing ratios versus averaging time τ. The dashed lines represent slopes for white noise, linear drifting and non-linear drifting.

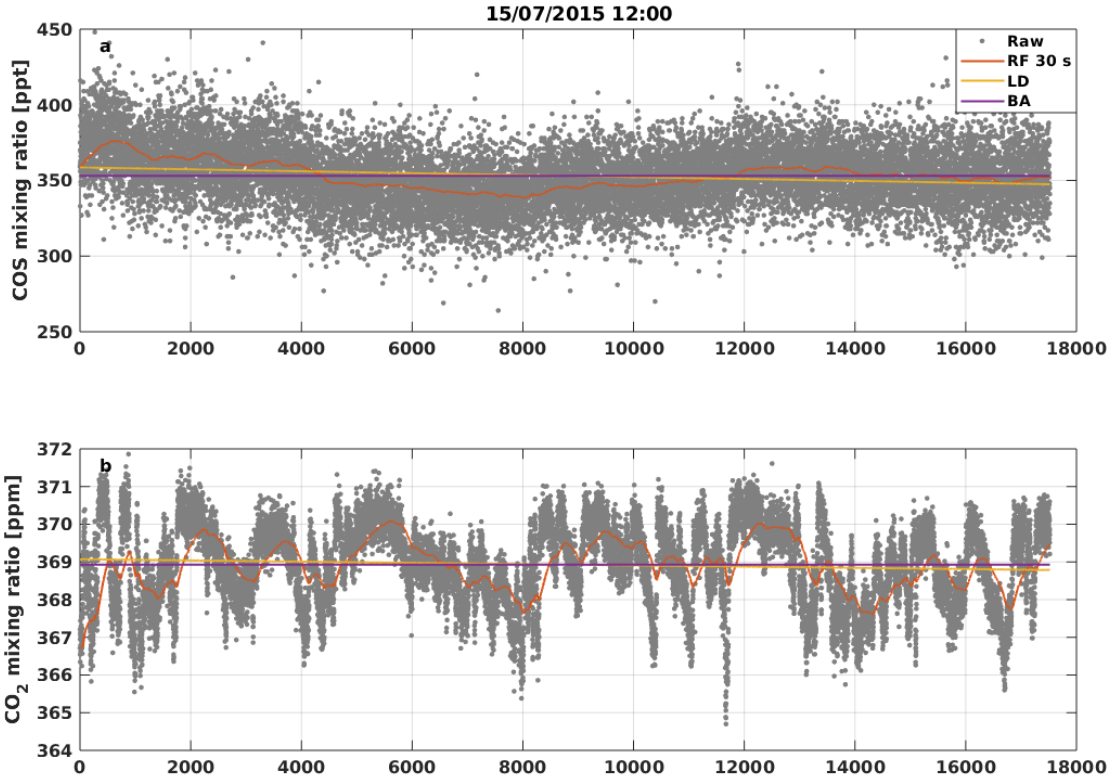

Figure S5. Comparison of different detrending methods (recursive filtering with 30 s averaging window, linear detrending and block averaging) applied to raw COS (a) and CO_2 (b) mixing ratio data on 15 July 2015 12:00--12:30.

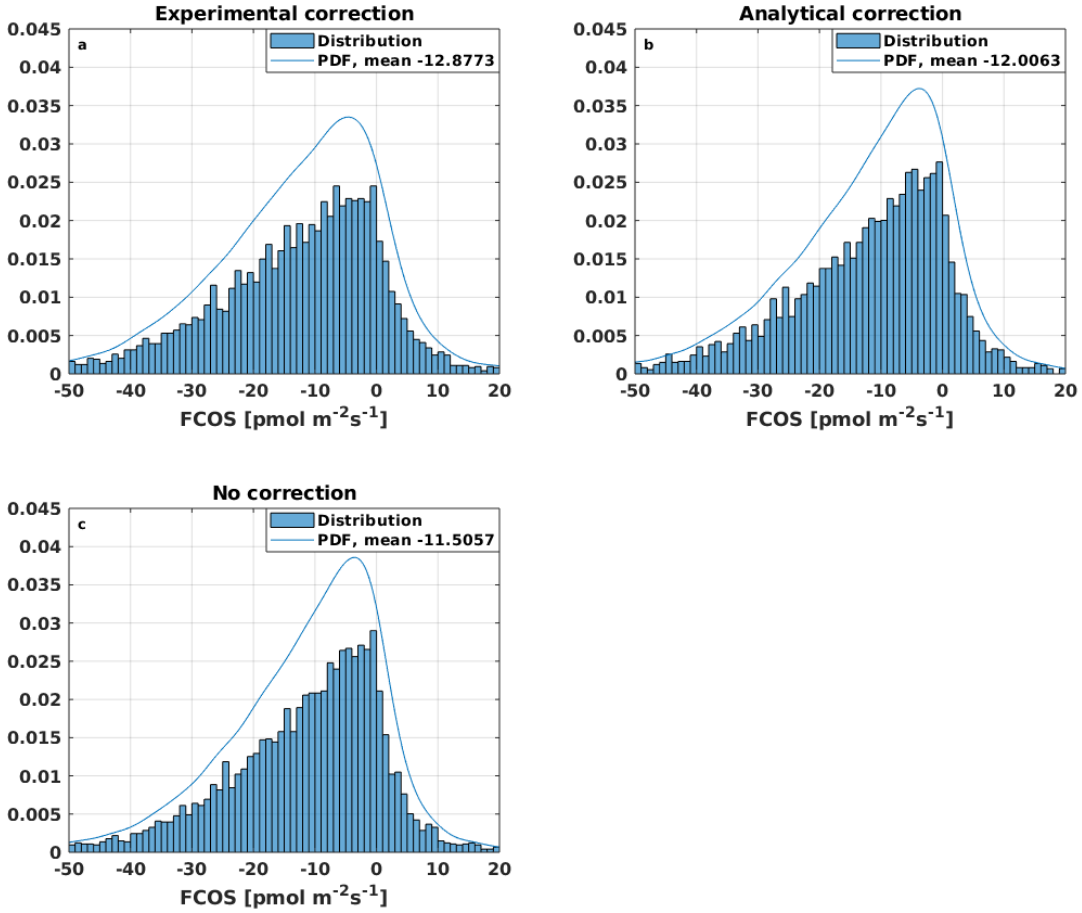

Figure S6. Histograms and PDFs of COS fluxes processed with experimental (a) and analytical (b) high-frequency spectral corrections or without any spectral corrections (c).

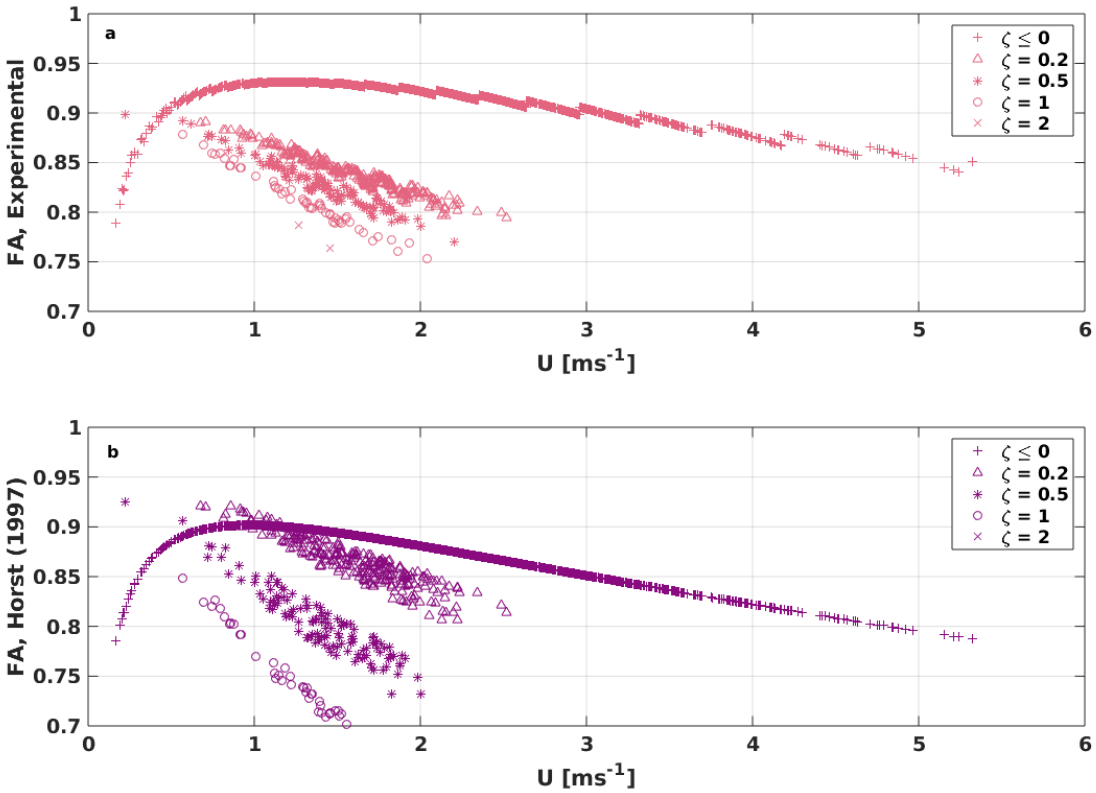

Figure S7. Flux attenuation versus wind speed in different stability classes for experimental (a) and analytical (b) high-frequency spectral correction methods.

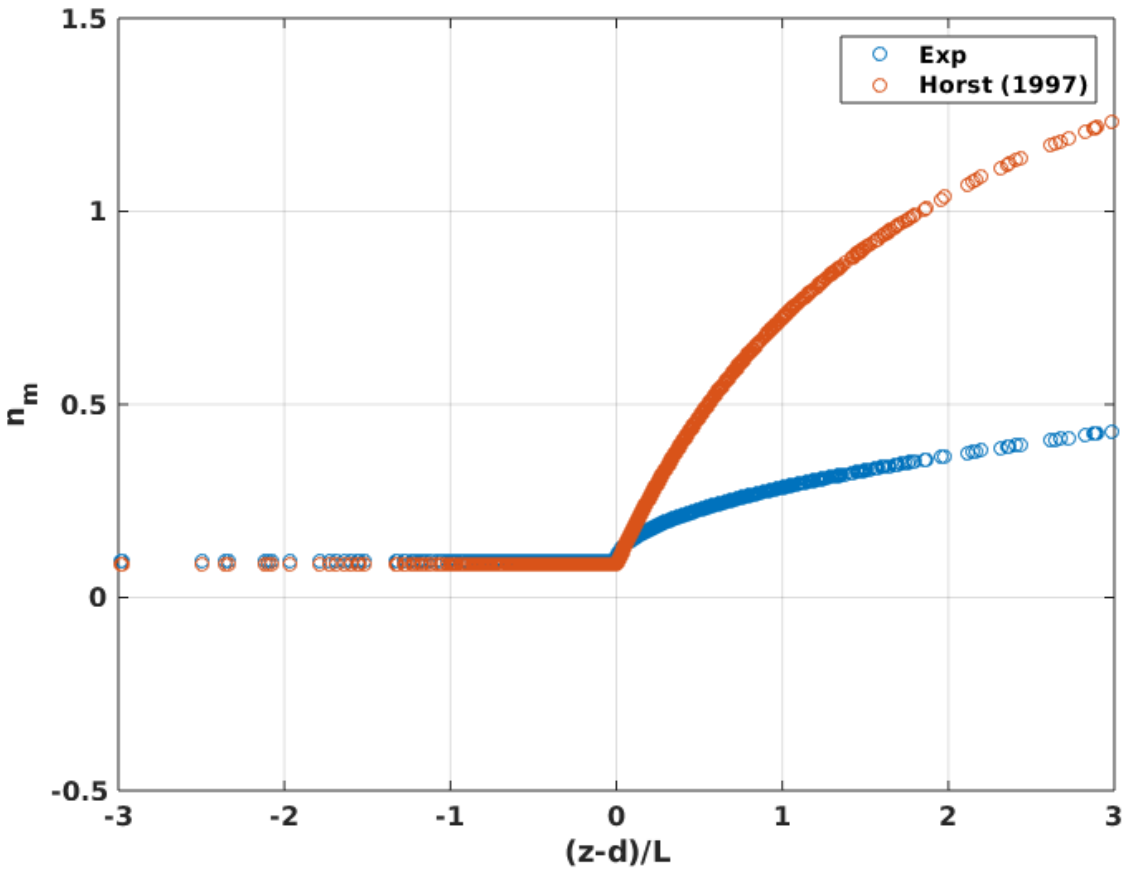

Figure S8. Cospectral peak frequency as a function of stability according to experimental method and analytical method by Horst (1997).

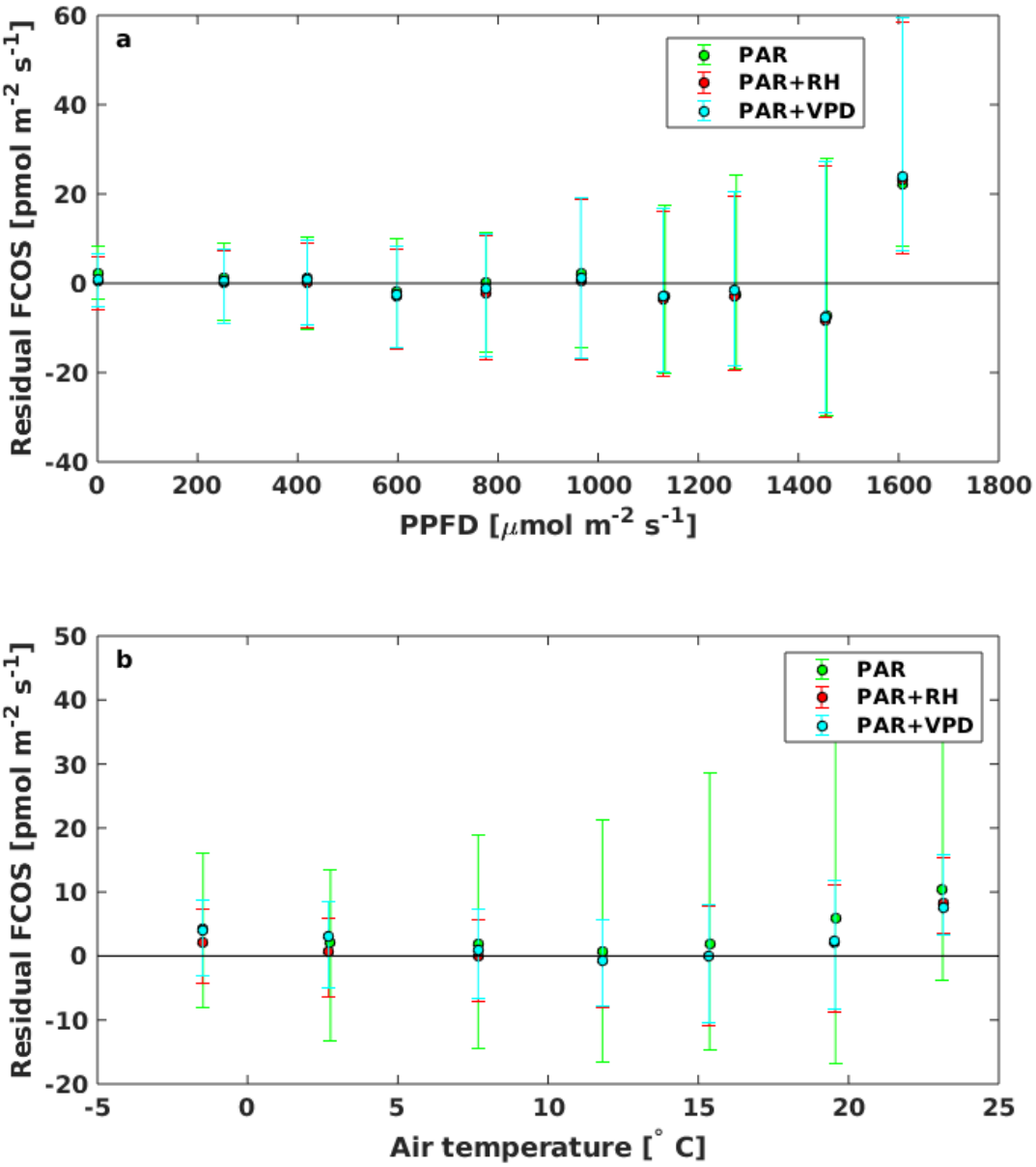

Figure S9. Median residuals and 25th and 75th percentiles of the different gap-filling methods against PAR (a) and air temperature (b), binned to 10 and 7 bins at equal distances, respectively. The different gap-filling methods are: gap-filling with only saturating PAR function (green), saturating PAR and linear dependency on RH (red) and saturating PAR and linear dependency on VPD (blue). Residuals calculated for the whole measurement period from 26 June to 31 October 2015.

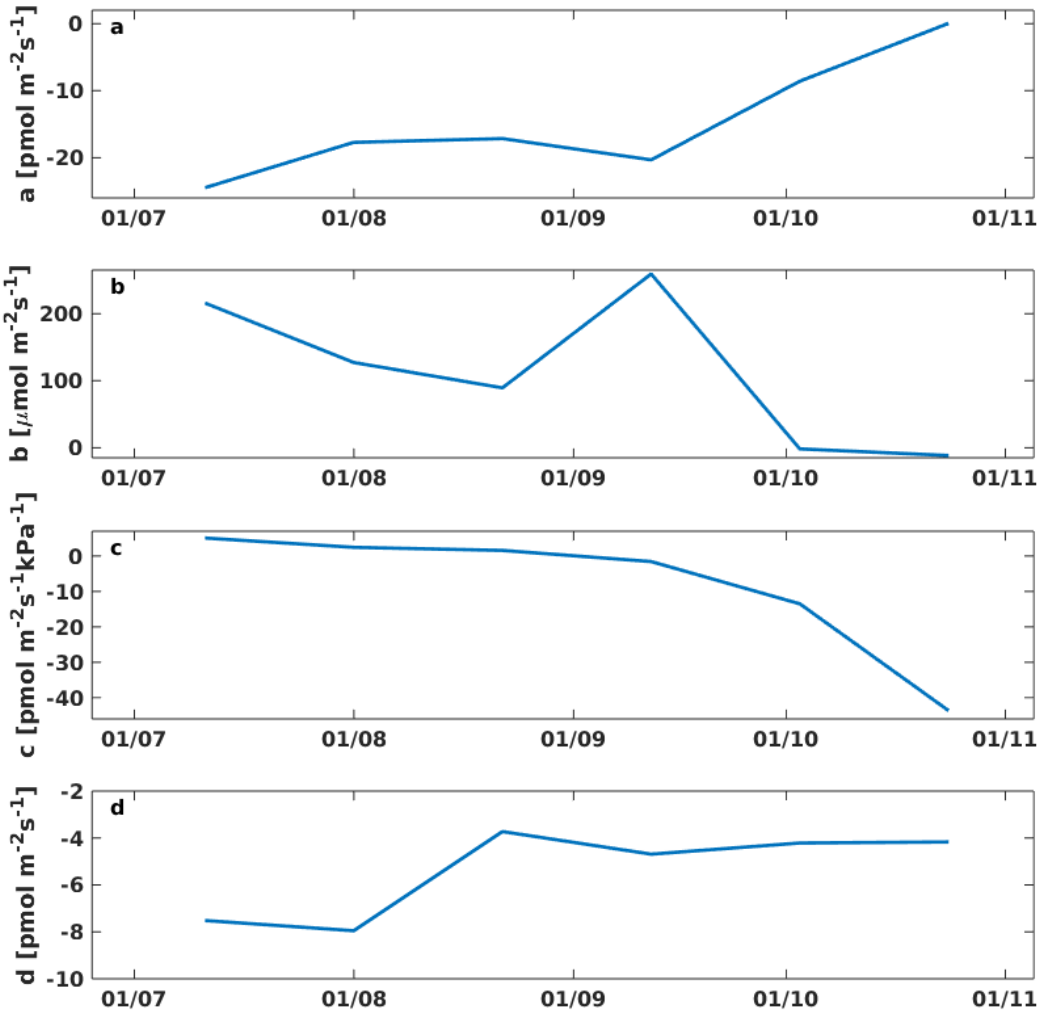

Figure S10. Time series of gap-filling parameters a, b, c and d.

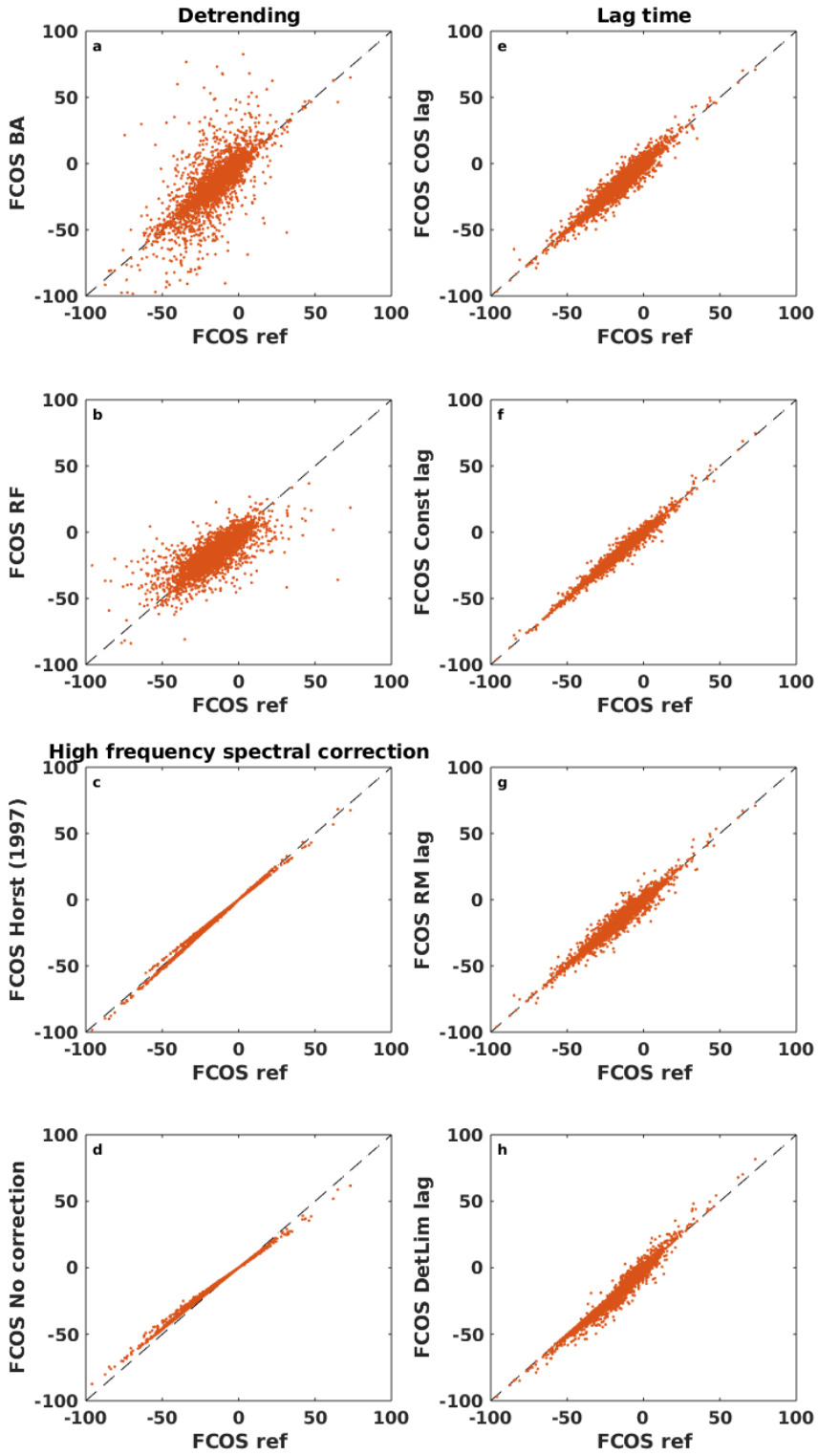

Figure S11. COS fluxes from different processing schemes against the reference flux. Subplots a-b represent different detrending options, subplots c-d different high-frequency spectral correction options and subplots e-h different lag time methods.